ISSN 0020-1685, Inorganic Materials, 2017, Vol. 53, No. 3, pp. 326–332. © Pleiades Publishing, Ltd., 2017.
Original Russian Text © B.A. Lineva, S.D. Kobylyanskaya, L.L. Kovalenko, O.I. V'yunov, A.G. Belous, 2017, published in Neorganicheskie Materialy, 2017, Vol. 53, No. 3, pp. 315–321.

Effect of Impurities on the Electrical Properties of the Defect Perovskite $Li_{0.33}La_{0.57}TiO_3$

B. A. Lineva*, S. D. Kobylyanskaya, L. L. Kovalenko, O. I. V'yunov, and A. G. Belous

Vernadsky Institute of General and Inorganic Chemistry, National Academy of Sciences of Ukraine, pr. Akademika Palladina 32/34, Kyiv, 03680 Ukraine

**e-mail: bozhena321@gmail.com*

Received May 10, 2016; in final form, September 16, 2016

Abstract—A perovskite phase with the composition $Li_{0.33}La_{0.57}TiO_3$ modified with up to 7 wt % Bi_2O_3, SiO_2, Li_3PO_4, or Li_3BO_3 has been prepared by solid-state reactions. The samples in the LLTO–Li_3PO_4, LLTO–Bi_2O_3, and LLTO–SiO_2 systems were single-phase over the entire composition range studied. In the LLTO–Li_3BO_3 system, increasing the lithium borate concentration causes a transition from a defect perovskite structure to the layered perovskite-related structure of $Li_2La_2Ti_3O_{10}$. The addition of Bi_2O_3 and Li_3PO_4 has been shown to increase the total conductivity of the ceramics by almost one order of magnitude. Li_3BO_3, Li_3PO_4, Bi_2O_3, and SiO_2 additives improve the sintering behavior of the $Li_{0.33}La_{0.57}TiO_3$ ceramics.

Keywords: ionic conductivity, grain-boundary conductivity, bulk conductivity, $Li_{3x}La_{(2/3)-x}\square_{(1/3)-2x}TiO_3$ perovskite, Schottky barrier, conductor, dielectric

DOI: 10.1134/S0020168517030074

INTRODUCTION

Lithium-ion-conducting materials are of great interest because they are potential candidates for use as electrolytes and electrodes in batteries for memory devices, displays, sensors, etc. [1, 2]. It is known that the basic requirements for electrolytes are high ionic conductivity, low electronic conductivity, chemical and electrochemical stability, safety, and a wide operating temperature range [3, 4]. Low ionic conductivity is a major obstacle to the commercialization of inorganic solid electrolytes.

At present, promising crystalline inorganic lithium-ion solid electrolytes include lithium lanthanum titanates with a defect perovskite structure, $Li_{3x}La_{(2/3)-x}\square_{(1/3)-2x}TiO_3$ (LLTO) ($0 < x < 0.16$) [5]. The $x = 0.11$ material possesses high room-temperature ionic conductivity: $\sigma \sim 10^{-7}$ to 10^{-4} S/cm (E_a = 0.3–0.4 eV). Its high ionic conductivity is due to the presence of A-site vacancies, which are responsible for lithium ion transport [6]. Ionic conduction is ensured by Li^+ ion motion through the vacancies. The grain-boundary conductivity of LLTO is known to be two orders of magnitude higher than its bulk conductivity [7, 8]. It is, therefore, important to improve its grain-boundary conductivity. Grain boundaries always have higher defect density than does the grain bulk. Because of the considerable defect density, there is a surface potential barrier, referred to as a Schottky barrier [9, 10]. It is known that an applied electric field can reduce the Schottky barrier. The interface in a conductor–dielectric system has a space charge, which can reduce the Schottky barrier. In theoretical studies [9, 10], Maier evaluated the effect of space charge on the height of Schottky barriers in M–MX conductor–dielectric systems. His results suggest the possibility of raising the grain-boundary conductivity.

As shown by Liang et al. [11], coating LiI grains with an α-Al_2O_3 dielectric layer considerably increases their electrical conductivity. However, we have found no reports on such studies for lithium ion conducting oxide systems. It is, therefore, of interest to investigate a lithium ion oxide conductor (LLTO)/dielectric (SiO_2) system. It is also possible to choose a dielectric additive with a low melting point (Bi_2O_3). Given that grain-boundary defects originate to a significant degree from lithium oxide vaporization during high-temperature sintering, it is of interest to use lithium-containing low-conductivity additives capable of lowering the sintering temperature, for example, Li_3BO_3 and Li_3PO_4.

The purpose of this work was to study the effect of Bi_2O_3, SiO_2, Li_3BO_3, and Li_3PO_4 additions on the microstructure and electrical properties of $Li_{0.33}La_{0.57}TiO_3$ with a defect perovskite structure.

EXPERIMENTAL

Synthesis of LLTO powder. LLTO defect perovskite powder was prepared by solid-state reaction. The synthesis procedure was described in detail elsewhere [5].

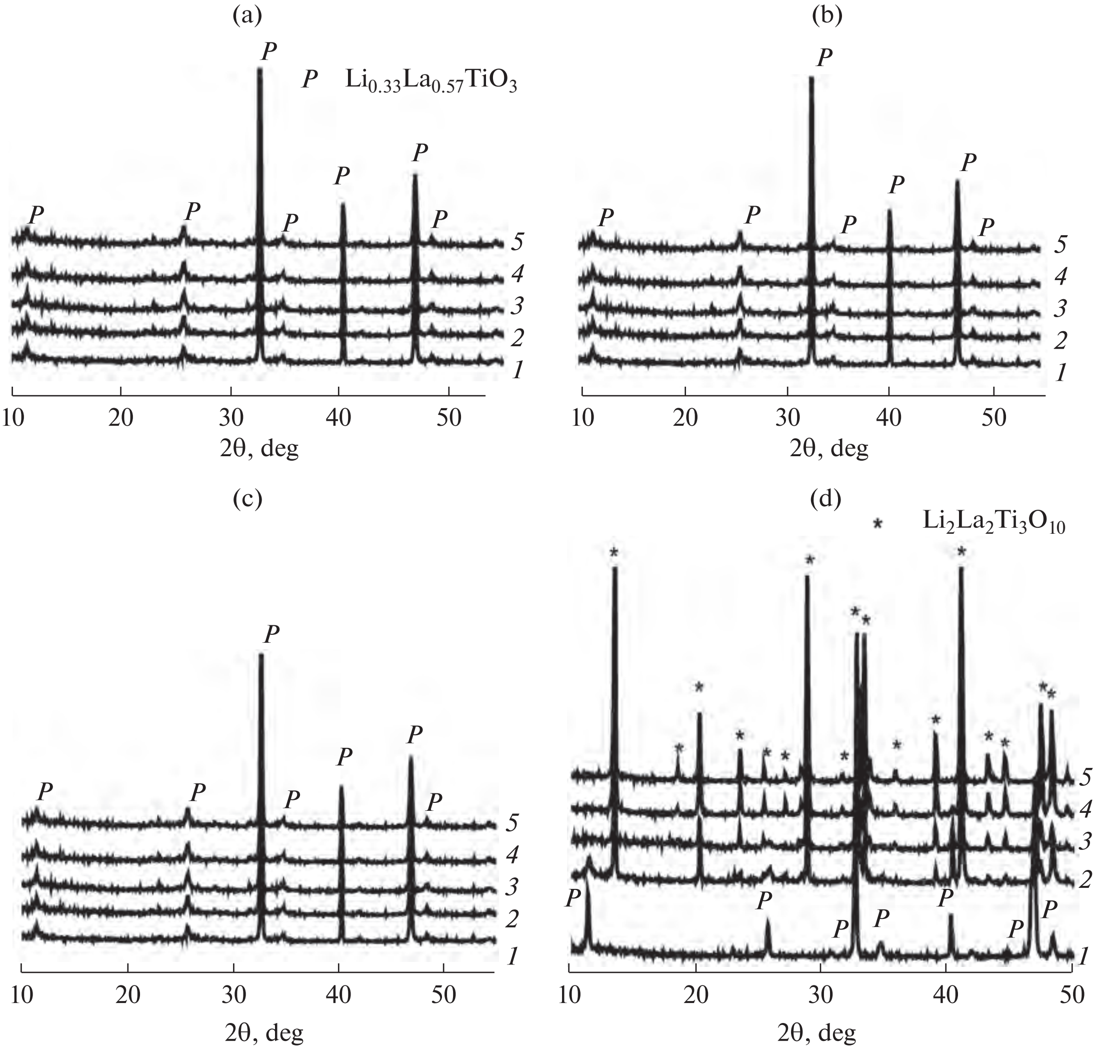

Fig. 1. Portions of X-ray diffraction patterns of (a) LLTO–Bi_2O_3, (b) LLTO–SiO_2, (c) LLTO–Li_3PO_4, and (d) LLTO–Li_3BO_3 ceramics containing (*1*) 0, (*2*) 1, (*3*) 3, (*4*) 5, and (*5*) 7 wt % additives.

The starting chemicals used were extrapure-grade lithium carbonate (Li_2CO_3), LO-1 lanthanum oxide (La_2O_3), and extrapure-grade titanium dioxide (TiO_2). The lithium carbonate and lanthanum oxide powders were first dried for 4 h at temperatures of 350 and 850°C, respectively, to remove residual water and absorbed CO_2. Immediately after drying, the powders were weighed. The resultant mixture was for 2 h with zirconium balls and then heat-treated at a temperature of 850°C for 4 h. After additional milling, the mixture was reacted at 1050°C for 2 h. The resultant single-phase material was ground in a planetary mill for 4 h at 650 rpm.

Synthesis of LLTO–Bi_2O_3 samples. To prepare LLTO–Bi_2O_3 samples, bismuth oxide was predried at a temperature of 600°C [12]. The synthesized LLTO powders were mixed with Bi_2O_3 (1, 3, 5, and 7 wt %).

Synthesis of LLTO–SiO_2 samples. The synthesized LLTO powders were coated with a SiO_2 layer [13]. To activate the grain surface, wet LLTO powder was stirred for 2 h using a mixture of tetrachloromethane (CCl_4) and ammonia as a dispersion medium. Next, reagent-grade tetraethyl orthosilicate, $Si(C_2H_5O)_4$, was added and the suspension was stirred for 10 h. The resultant mixture was dried at 150°C. We prepared LLTO samples containing 1, 3, 5, and 7 wt % SiO_2.

Synthesis of LLTO–Li_3PO_4 samples. Lithium orthophosphate, Li_3PO_4, was presynthesized by neutralizing orthophosphoric acid, H_3PO_4, with an excess of a saturated reagent-grade LiOH solution. The resultant precipitate was dried at a temperature of 150°C for 5 h and then calcined at t = 650°C for 2 h. The LLTO powders were mixed with 1, 3, 5, and 7 wt % Li_3PO_4.

Synthesis of LLTO–Li_3BO_3 samples. Lithium borate, Li_3BO_3, was prepared as described by Shingo

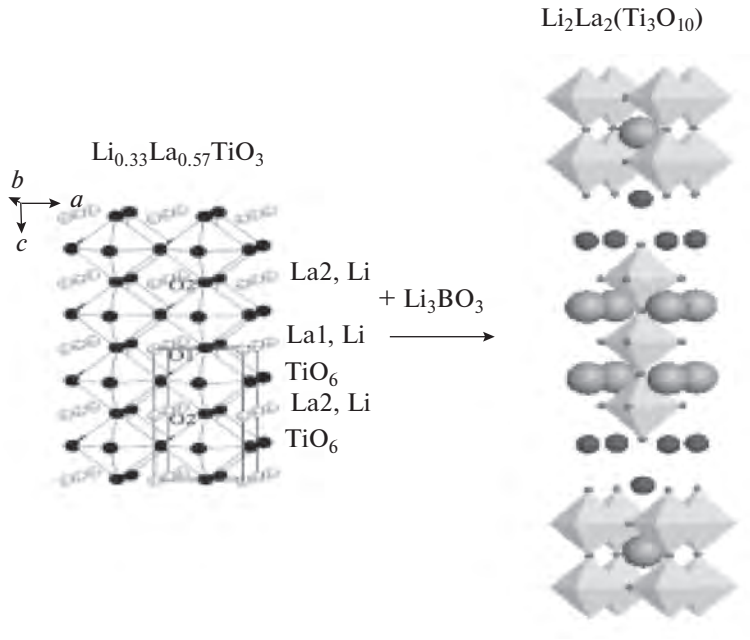

Fig. 2. Schematic illustrating the transition from the defect perovskite structure of $Li_{0.33}La_{0.57}TiO_3$ to the layered perovskite-related structure of $Li_2La_2Ti_3O_{10}$.

Ohta et al. [16]. A 2 : 3 mixture of analytical-grade boric acid (H_3BO_3) and extrapure-grade lithium carbonate was reacted in a platinum crucible at $t = 850$°C for 10 h. The resultant lithium borate, Li_3BO_3, was mixed with the LLTO powder (1, 3, 5, and 7 wt % Li_3BO_3).

The LLTO–Bi_2O_3, LLTO–SiO_2, LLTO–Li_3BO_3, and LLTO–Li_3PO_4 samples were homogenized by grinding in a vibratory mill under ethanol and dried. After that, an aqueous 5% poly(vinyl alcohol) solution was added. After pressing ($d = 14$ mm, $p = 80$ MPa), the compacts were isothermally heat-treated at temperatures in the range 1120–1230°C for 4 h.

X-ray powder diffraction patterns were collected on a DRON-4-07 X-ray diffractometer (Ni-filtered CuK_α radiation) in the angular range $2\theta = 10°$–$150°$ with a scan step of $\pm 0.04°$ and a counting time per data point of 6 s. As external standards, we used SiO_2 (2θ calibration) and Al_2O_3 (intensity standard).

The microstructures of the polycrystalline samples were examined on a scanning electron microscope (SEM) (JEOL JSM-6490LV, Japan) equipped with an INCAEnergy+ integrated electron probe analysis system based on energy- and wavelength-dispersive spectrometers (EDS + WDS, Oxford Instruments, United Kingdom) and with an HKL Channel detector (Oxford Instruments).

In electrical measurements, we used 1.5-mm-thick samples. Silver metal contacts were made by firing silver paste (Duponte, USA) at 600°C. Impedance measurements were performed in the range from 100 Hz to 1 MHz in dry air using a 1260 A impedance/gain phase analyzer (Solartron Analytical, United Kingdom).

RESULTS AND DISCUSSION

Bi_2O_3, Li_3PO_4, and Li_3BO_3 are known to have low melting points: 825, 837, and 840°C, respectively. Accordingly, these additives made it possible to reduce the sintering temperature of ceramics by 60°C in the case of the LLTO–Bi_2O_3 and LLTO–Li_3BO_3 systems (from 1230 to 1170°C) and by 110°C in the case of the LLTO–Li_3PO_4 system (from 1230 to 1120°C). In the LLTO–SiO_2 system, the sintering temperature of ceramics remained unchanged because of the high melting point of SiO_2 (1728°C).

Figure 1 shows X-ray diffraction patterns of the LLTO samples containing Bi_2O_3, SiO_2, Li_3PO_4, and Li_3BO_3 additions after sintering at various temperatures. In the composition range studied (<=7 wt %), the LLTO–Bi_2O_3 (Fig. 1a), LLTO–SiO_2 (Fig. 1b), and LLTO–Li_3PO_4 (Fig. 1c) samples are single-phase: there are only reflections from a perovskite phase.

In the case of LLTO with Li_3BO_3 additions (Fig. 1d), the amount of the layered perovskite phase $Li_2La_2Ti_3O_{10}$ increases with increasing lithium borate concentration and the sample containing 9 wt % Li_3BO_3 consists of $Li_2La_2Ti_3O_{10}$ and trace levels of TiO_2. The formation of a layered perovskite compound which is the third member ($n = 3$) of an $A_{n+1}Ti_nO_{3n+1}$ Ruddlesden–Popper series can be thought of (Fig. 2) as

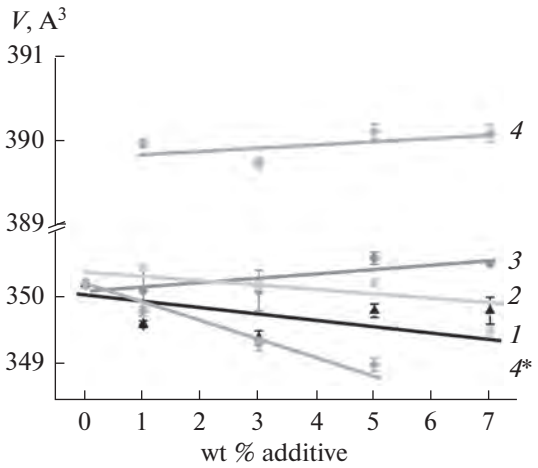

Fig. 3. Unit-cell volume as a function of additive concentration in the (*1*) LLTO–Bi_2O_3, (*2*) LLTO–SiO_2, (*3*) LLTO–Li_3PO_4, and (*4*) LLTO–Li_3BO_3 systems; (*4**) layered perovskite phase.

the incorporation of lithium ions into every third layer of TiO_6 octahedra in the perovskite structure, which is accompanied by the generation of considerable mechanical stress in these layers. The mechanical stress leads to breaking of some bonds in the layers of TiO_6 octahedra [17], the formation of octahedron chains in the layered perovskite structure [17], and partial precipitation of TiO_2 as a second phase according to the scheme

$$\begin{aligned}\mathrm{Li}_{3x}\mathrm{La}_{(2/3)-x}\mathrm{TiO}_3 + 2/3(1/3-2x)\mathrm{Li}_3\mathrm{BO}_3 \\ = (2-3x)/6\mathrm{Li}_2\mathrm{La}_2\mathrm{Ti}_3\mathrm{O}_{10} + 3/2x + \mathrm{TiO}_2 \\ + 1/3(1/3-2x)\mathrm{B}_2\mathrm{O}_3.\end{aligned}$$

The structural parameters of all the LLTO samples containing Bi_2O_3, SiO_2, Li_3PO_4, and Li_3BO_3 additions were determined by the Rietveld profile analysis method (Fig. 3). The results demonstrate that the unit-cell volume decreases with increasing Bi_2O_3 (Fig. 3, line *1*), Li_3PO_4 (Fig. 3, line *3*), and Li_3BO_3 (Fig. 3, line *4*) concentrations. In the case of SiO_2 additions (Fig. 3, line *2*), the unit-cell volume increases because raising the temperature leads to the formation of a TiO_2/SiO_2 layer on the sample surface. This gives rise to deviations from stoichiometry in the inner structure because of the decrease in lithium concentration and the increase in lanthanum concentration. Accordingly, the total conductivity decreases.

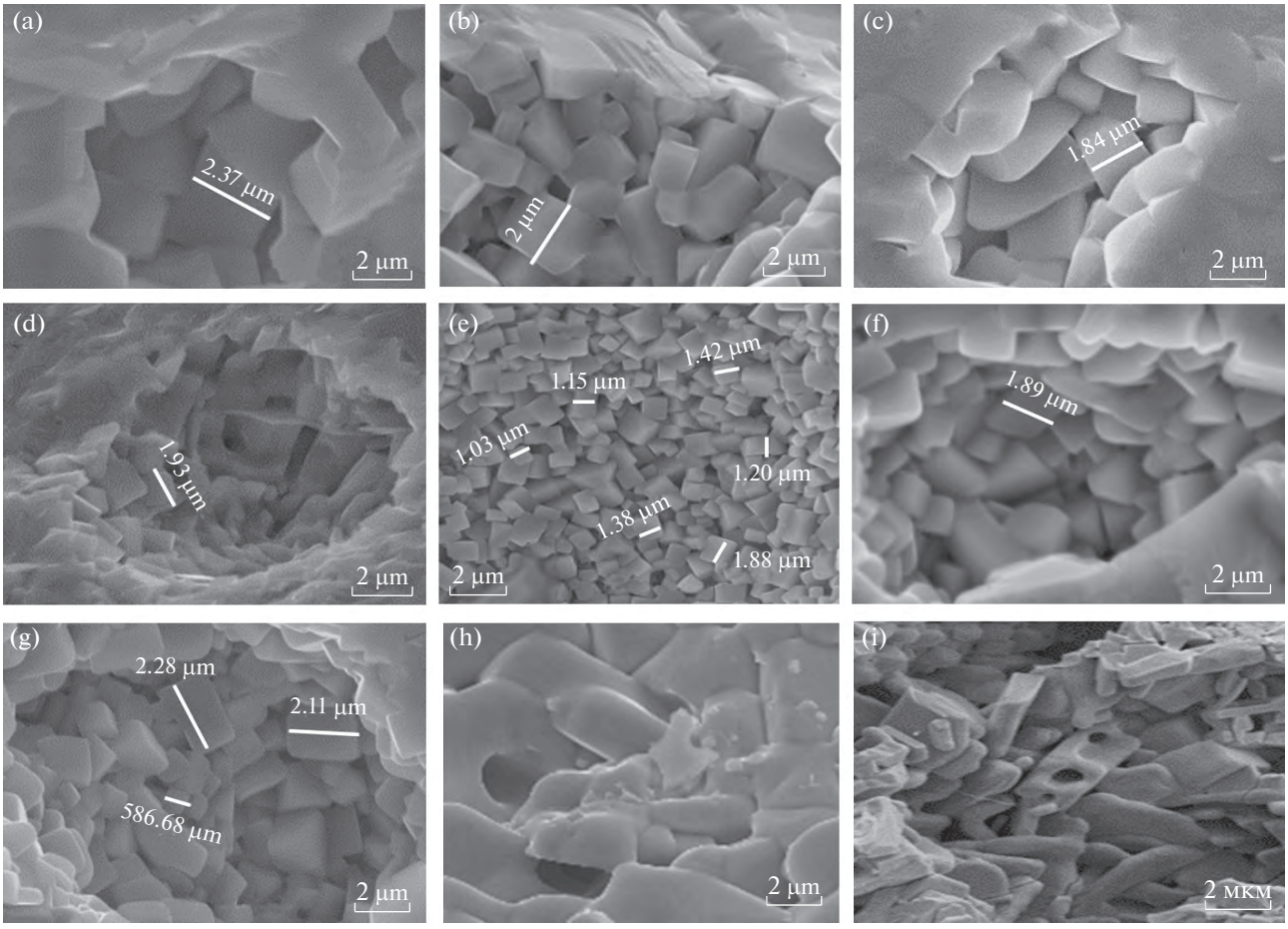

Fig. 4. Micrographs of the (a) LLTO, (b) LLTO–Bi_2O_3 (3%), (c) LLTO–Bi_2O_3 (7%), (d) LLTO–SiO_2 (3%), (e) LLTO–SiO_2 (7%), (f) LLTO–Li_3PO_4 (1%), (g) LLTO–Li_3PO_4 (5%), (h) LLTO–Li_3BO_3 (1%), and (i) LLTO–Li_3BO_3 (3%) ceramics.

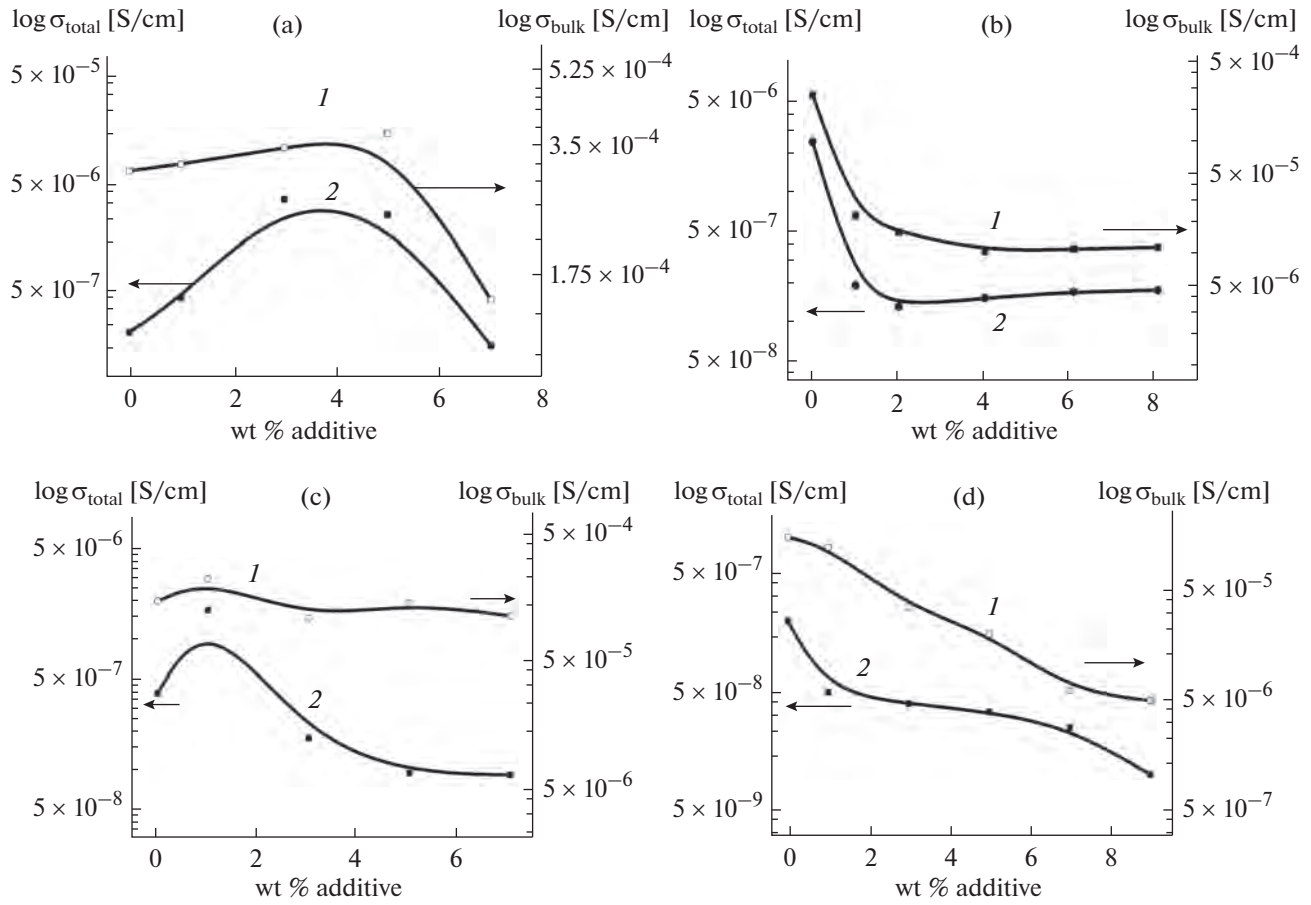

Fig. 5. (*1*) Bulk conductivity and (*2*) total conductivity as functions of additive concentration in the (a) LLTO–Bi_2O_3, (b) LLTO–SiO_2, (c) LLTO–Li_3PO_4, and (d) LLTO–Li_3BO_3 systems.

Figure 4 shows micrographs of $Li_{0.33}La_{0.57}TiO_3$ ceramics without additives and with different concentrations of Bi_2O_3 (3 and 7 wt %), SiO_2 (3 and 7 wt%), Li_3PO_4 (1 and 5 wt %), and Li_3BO_3 (1 and 7 wt %). The addition of Bi_2O_3 (Figs. 4b, 4c), SiO_2 (Figs. 4d, 4e), and Li_3PO_4 (Figs. 4f, 4g) leads to changes in the microstructure of the LLTO perovskite material. Increasing their concentration increases the density of the material. Moreover, the average grain size decreases with increasing additive concentration: from ~2–2.5 μm in the additive-free material to 500 nm at 7 wt % additives. In the LLTO–Li_3BO_3 system, the grains were platelike in shape (Figs. 4h, 4i).

Figure 5 shows composition dependences of room-temperature electrical conductivity for LLTO containing various concentrations of the additives. In the LLTO–Bi_2O_3 system, increasing the bismuth oxide content from 0 to 3 wt % increases the total conductivity (σ_{total}) of the materials by almost one order of magnitude, from 8×10^{-7} to 6×10^{-6} S/cm (Fig. 5a, curve *2*), whereas the bulk conductivity (σ_{bulk}) remained unchanged ($3 \pm 0.2 \times 10^{-4}$ S/cm) (Fig. 5a, curve *1*). Since the total conductivity of a material depends on both its bulk conductivity and its grain-boundary conductivity, the increase in total conductivity on the addition of 3 wt % Bi_2O_3 can be tentatively attributed to the increase in grain-boundary conductivity because of the decrease in Schottky barrier height. Further increasing the Bi_2O_3 content (from 3 to 7 wt %) reduces both the total conductivity and bulk conductivity, to 3×10^{-8} and 1.6×10^{-4} S/cm, respectively.

In the LLTO–SiO_2 system, increasing the additive concentration (from 0 to 8 wt %) reduces both the total conductivity (from 2.3×10^{-6} to 1.75×10^{-7} S/cm) and bulk conductivity (from 2.58×10^{-4} to 1×10^{-5} S/cm) (Fig. 5b). This suggests that the addition of silicon dioxide leads to blocking of Li^+ ion motion.

In the LLTO–Li_3PO_4 system, the total conductivity passes through a maximum, like that in the LLTO–Bi_2O_3 system. The addition of 1 wt % lithium phosphate (Fig. 5c, curve *2*) increases the total conductivity of the material from 7×10^{-7} to 3×10^{-6} S/cm, whereas the bulk conductivity remains unchanged: $\sigma_{bulk} = (2 \pm 0.25) \times 10^{-4}$ S/cm (Fig. 5c, curve *1*). Like

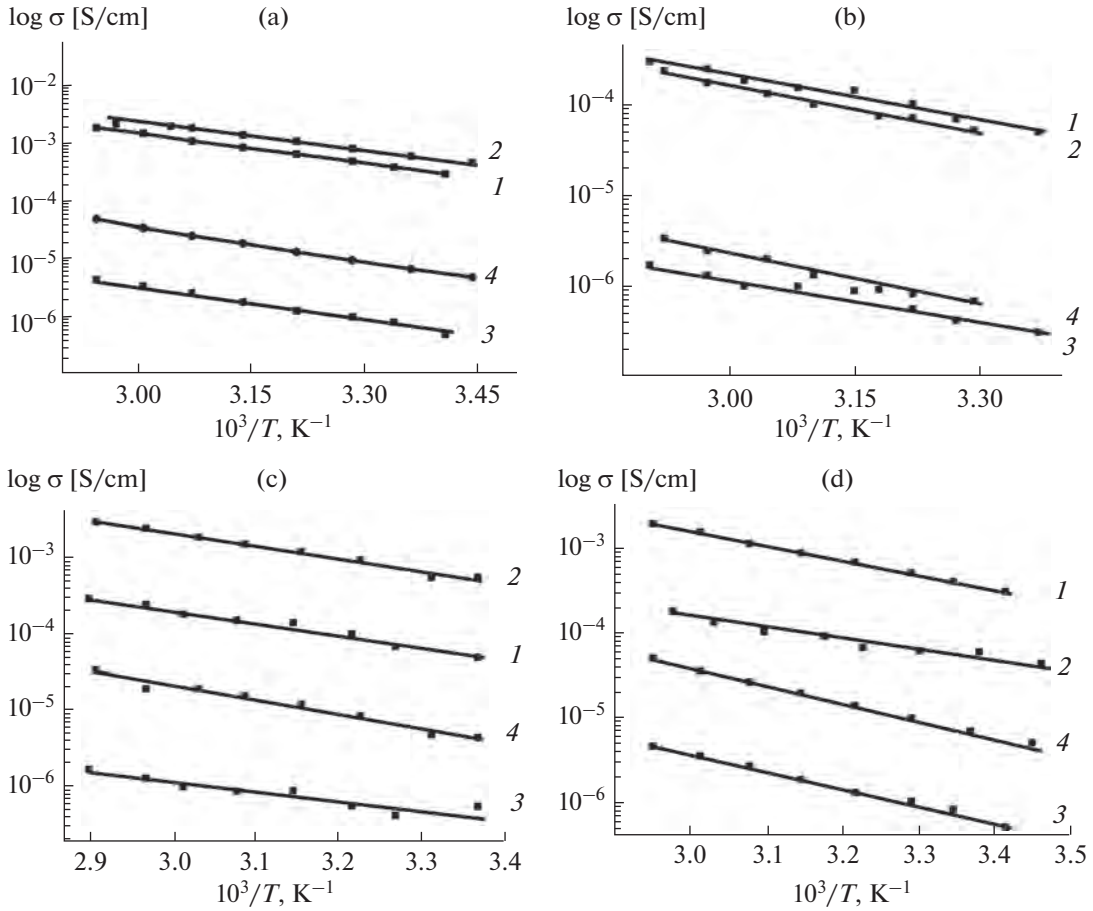

Fig. 6. Arrhenius plots of (*1*, *2*) bulk conductivity and (*3*, *4*) total conductivity for the (a) LLTO–Bi_2O_3, (b) LLTO–SiO_2, (c) LLTO–Li_3PO_4, and (d) LLTO–Li_3BO_3 systems; (*1*, *3*) no additive, (*2*, *4*) 3 wt % additive.

in the case of LLTO–Bi_2O_3, the increase in grain-boundary conductivity is attributable to a decrease in the height of Schottky barriers on the addition of ≤1 wt % Li_3PO_4.

In the LLTO–Li_3BO_3 system (Fig. 5d), both the bulk conductivity and total conductivity decrease with increasing lithium borate concentration (σ_{bulk} from 2.2×10^{-4} to 4×10^{-5} S/cm and σ_{total} from 7.5×10^{-7} to 4×10^{-8} S/cm). The reason for this is that the electrical conductivity of the layered perovskite phase is lower than that of the defect perovskite.

The activation energy E_a was evaluated from temperature dependences of electrical conductivity for the ceramics containing various percentages of Bi_2O_3, SiO_2, Li_3PO_4, and Li_3BO_3 (Fig. 6). The activation energy for bulk ionic conduction was determined to be 0.33–0.34 eV, and that for total conduction (grain-boundary and bulk conductivity), 0.39–0.40 eV. These values are typical of lithium-ion conductors [18] and are insensitive to the additives. This strongly suggests that the additives are not incorporated into the structure of LLTO.

CONCLUSIONS

A perovskite phase with the composition $Li_{0.33}La_{0.57}TiO_3$ modified with various concentrations of Bi_2O_3, SiO_2, Li_3PO_4, and Li_3BO_3 has been prepared by solid-state reactions. The samples in the LLTO–Li_3PO_4, LLTO–Bi_2O_3, and LLTO–SiO_2 systems were single-phase over the entire composition range studied. In the case of LLTO–Li_3BO_3, the additive causes a transition from the defect perovskite structure to the layered perovskite-related structure of $Li_2La_2Ti_3O_{10}$.

Small amounts of the additives have been shown to lower the sintering temperature from 1230 to 1170°C in the LLTO–Bi_2O_3 and LLTO–Li_3BO_3 systems and from 1230 to 1120°C in the LLTO–Li_3PO_4 system.

We were able to raise the total conductivity of the LLTO–Bi_2O_3 and LLTO–Li_3PO_4 systems by almost one order of magnitude, to $\sigma_{total} = 6 \times 10^{-6}$ and 3×10^{-6} S/cm, respectively, whereas the bulk conductivity remained unchanged. This can be tentatively accounted for in terms of an increase in grain-boundary conductivity due to a reduction in the height of Schottky barriers.

REFERENCES

1. Kobayashi, Y., Miyashiro, H., Takeuchi, T., et al., All-solid-state lithium secondary battery with ceramic/polymer composite electrolyte, *Solid State Ionics,* 2002, vol. 3, pp. 137–142.
2. Brousse, T., Fragnaud, P., Marchand, R., et al., All oxide solid-state lithium-ion cells, *J. Power Sources,* 1997, vol. 68, pp. 412–415.
3. Knauth, P., Inorganic solid Li-ion conductors: an overview, *Solid State Ionics,* 2009, vol. 180, pp. 911–916.
4. Belous, A., Pashkova, E., Gavrilenko, O., et al., Solid electrolytes based on lithium-containing lanthanum metaniobates, *J. Eur. Ceram. Soc.,* 2004, vol. 24, pp. 1301–1304.
5. Belous, A., Yanchevskiy, O., V'yunov, O., Bohnke, O., et al., Peculiarities of $Li_{0.5}La_{0.5}TiO_3$ formation during the synthesis by solid-state reaction or precipitation from solution, *Chem. Mater.,* 2004, vol. 16, pp. 407–417.
6. Herrero, C.P., Varez, A., Rivera, A., et al., Influence of vacancy ordering on the percolative behavior of $(Li_{1-x}Na_x)_{3y}La_{2/3-y}TiO_3$ perovskites, *J. Phys. Chem.,* 2005, vol. 109, no. 8, pp. 3262–3268.
7. Sanjuan, M.L., Laguna, M.A., Belous, A.G., et al., On the local structure and lithium dynamics of $Li_{0.5}(Li,Na)_{0.5}TiO_3$ ionic conductor. A Raman study, *Chem. Mater.,* 2005, vol. 17, pp. 5862–5866.
8. Bohnke, O., Bohnke, C., and Fourquet, J.L., Mechanism of ionic conduction and electrochemical intercalation of lithium into the perovskite lanthanum lithium titanate, *Solid State Ionics,* 1996, vol. 91, pp. 21–31.
9. Maier, J., Defect chemistry and ion transport in nanostructured materials. Part II. Aspect of nanoionics, *Solid State Ionics,* 2003, vol. 157, pp. 327–334.
10. Maier, J., Influence of interface structure on mass transport, *Solid State Ionics,* 1988, vols. 28–30, pp. 1073–1077.
11. Liang, C.C., Joshi, A.V., and Hamilton, N.E., Solid-state storage batteries, *J. Appl. Electrochem.,* 1978, vol. 8, pp. 445–454.
12. Martínez-Sarrión, M.-L., Mestres, L., Herráiz, M., Maqueda, O., Bakkali, A., and Fernández, N., Phase diagram and impedance spectroscopy study of the $La_{0.5+x-y}Bi_yLi_{0.5-3x}TiO_3$ system, *Eur. J. Inorg. Chem.,* 2002, vol. 7, pp. 1794–1800.
13. Kiyoharu Tadanada, Ryohei Takano, and Takahino Ichinose, Coating and water permeation properties of SiO_2 thin films prepared by the sol–gel method on Nylon-6 substrates, *Electrochem. Commun.,* 2013, vol. 33, pp. 51–54.
14. Yaojun, A.Du. and Holzwarth, N.A.W., Li ion diffusion mechanisms in the crystalline electrolyte Li_3PO_4, *J. Electrochem. Sources,* 2007, vol. 154, pp. 999–1004.
15. Belous, A.G., V'yunov, O.I., Kovalenko, L.L., Bohnke, O., and Bohnke, C., Synthesis of thin-films electrodes based on LiPON and LiPON–LLTO–LiPON, *Russ. J. Electrochem.,* 2014, vol. 50, no. 6, pp. 584–591.
16. Shingo Ohta, Shogo Komagate, and Juntaro Seki, All-solid-state lithium ion battery using garnet-type oxide and Li_3BO_3 solid electrolytes fabricated by screen-printing, *J. Power Sources,* 2013, vol. 238, pp. 53–56.
17. Titov, Yu.O., Bilyavina, N.M., and Markov, V.Ya., New $A_nB_{n-1}O_{3n}$ layered compounds in $A^{II}_5B^{V}_4O_{15}$–ABO_3 systems, *Ukr. Khim. Zh.,* 2013, vol. 79, no. 1, pp. 13–17.
18. Šalkus, T., Kazakevičius, E., Kežionis, A., Orliukas, A.F., Badot, J.C., and Bohnke, O., Determination of the non-Arrhenius behaviour of the bulk conductivity of fast ionic conductors LLTO at high temperature, *Solid State Ionics,* 2011, vol. 88, pp. 69–72.

Translated by O. Tsarev

SPELL: 1. OK